Biomolecules and Biomedicine
ISSN: 2831-0896 (Print) | ISSN: 2831-090X (Online)

Journal Impact Factor® (2023): 3.1
CiteScore® (2023): 7.4
www.biomolbiomed.com | www.blog.bjbms.org

RESEARCH ARTICLE

Wang et al: ICD risk signature for CRC prognosis

Immunogenic cell death-related risk signature for tumor microenvironment profiling and prognostic prediction in colorectal cancer

Pengcheng Wang[1*], Wei Zhao[2], Linghong Guo[1], Hailei Cao[3]

[1]Colorectal Surgery, Shanxi Province Cancer Hospital/Shanxi Hospital Affiliated to Cancer Hospital, Chinese Academy of Medical Sciences/Cancer Hospital Affiliated to Shanxi Medical University, Taiyuan, China

[2]Department of Anesthesiology, The First Affiliated Hospital of Harbin Medical University, Harbin, China

[3]Department of Colorectal and Anal Surgery, Shanxi Province Cancer Hospital/ Shanxi Hospital Affiliated to Cancer Hospital, Chinese Academy of Medical Sciences/Cancer Hospital Affiliated to Shanxi Medical University, Taiyuan, China

[*]**Correspondence to:** Pengcheng Wang: wpch1021@126.com

DOI: https://doi.org/10.17305/bb.2025.12028

ABSTRACT

Immunogenic cell death (ICD) reshapes the tumor immune microenvironment and activates the adaptive immune response. However, the clinical significance of ICD-associated genes in colorectal cancer (CRC) remains unclear. In this study, we used weighted gene co-expression network analysis (WGCNA) to identify ICD-related gene modules. An ICD-related risk score (ICDRS) was then constructed using Cox regression modeling and LASSO analysis. Immune cell infiltration in patients with different risk levels was assessed using the ESTIMATE and ssGSEA algorithms. The OncoPredict package was employed to explore the association between the ICDRS and chemotherapy drug sensitivity. Finally, the expression levels of ICD-related genes were validated through in vitro cellular experiments. Three CRC prognostic genes—*CLMP*, *NRP1*, and *PLEKHO1*—were identified from a set of 34 ICD-associated genes based on WGCNA and LASSO analyses. These genes were used to construct the ICDRS model. Notably, a high ICDRS was found to be an independent predictor of poorer overall survival (OS) in CRC patients. High-risk patients also exhibited increased immune cell infiltration. Moreover, the ICDRS was significantly correlated with sensitivity to conventional chemotherapeutic drugs, suggesting its potential utility in guiding personalized chemotherapy. Cellular assays confirmed that *CLMP*, *NRP1*, and *PLEKHO1* were differentially expressed between normal and cancerous cells, and that *NRP1* specifically promoted the proliferation, migration, and invasion of CRC cells. In conclusion, the ICDRS may serve as a reliable predictor of CRC prognosis and offers a promising direction for the clinical management of CRC patients.

Keywords: Colorectal cancer; CRC; drug resistance; prognostic signature; immunogenic cell death; ICD; tumor immune microenvironment, TIME; cancer

INTRODUCTION

Colorectal cancer (CRC) ranks the third most frequently diagnosed type of cancer worldwide. The annual incidence of CRC reached 1.9 million cases, which represents roughly 10% of all newly diagnosed cancers all over the world. At present, there is a

rapid increase in the incidence of CRC among younger populations in both developed and developing regions [1, 2]. The evolution of CRC is an intricate process that encompasses several stages and the involvement of genes. CRC cells exhibit distinct biological behaviors, characterized by robust proliferation, susceptibility to relapse, and metastasis [3, 4]. Currently, the survival of CRC remains dismal [5-7], which requires the identification of novel prognostic, therapeutic, and diagnostic biomarkers for the cancer.

Immunogenic cell death (ICD) is a type of cell death [8, 9] in which the interaction between immune cells and dying cells could be considered as an effective communication between the immune system and dying cells [10]. The process of ICD involves apoptosis, during which damage associated molecular patterns (DAMPs) will be released from tumor cells. These DAMPs will be detected by NOD-like receptors (NLRs) and innate immune receptors like Toll-like receptors (TLRs) to stimulate immune reactions to specifically target the tumor. This will promote and also prolong the effectiveness of chemotherapy drugs through a dual mechanism of directly killing cancer cells and enhancing antitumor immune responses [11, 12]. Previous study developed and verified an ICD risk signature for lower-grade glioma using 12 ICD-associated genes by analyzing the expressions, functions, and genetic alterations of 34 ICD-associated genes [13]. Two ICD-associated subtypes were classified applying consensus clustering and an ICD-associated prognostic model was established to help predict the survival for patients suffering from head and neck squamous cell carcinoma [14]. In addition, single-cell analysis showed that in ascending thoracic aortic aneurysms, the target cells of the ICD were endothelial cells, in which the aortic endothelial cell receptor ACKR1 promoted the infiltration of T-cells and myeloid cells through CCL5 and CXCL8 ligands, respectively [15]. Hence, mining effective ICD-related biomarkers might improve the clinical outcomes for patients with CRC.

The role of immune system in cancer initiation, progression, and therapy has been extensively explored. Recent therapeutic studies highlighted the crucial interplay between dying or dead cancer cells and immune cells in determining cancer treatment efficacy [16]. ICD triggers both adaptive and innate immunological responses, helping

to form a long-lasting immunological memory [17-19]. Similarly, cancer therapies work to stimulate anticancer immune responses and form long-term anticancer immunity by inducing ICDs [20].

The aim of this study was to construct a risk scoring model based on ICD-related genes in order to evaluate its potential application in prognosis prediction, tumor immune microenvironment characterization, and personalized treatment guidance for CRC patients. This study established an ICD-related risk score (ICDRS) for patients with CRC based on genes correlated with ICD using weighted gene co-expression analysis (WGCNA) and validated the prognostic value and independent predictive performance of the ICDRS. Additionally, ICDRS-associated somatic mutation status and copy number alteration (CNA) were analyzed by molecular characterization. Furthermore, functional pathway alterations and immune infiltration were assessed. In conclusion, the ICDRS model we constructed can serve as a potential independent prognostic indicator for CRC patients and provide new biomarkers and potential therapeutic targets for precision immunotherapy and personalized chemotherapy regimens.

MATERIALS AND METHODS

Data acquisition and preprocessing

Bulk-sequencing data in the form of FPKM were log2-transformed. Survival data of 367 primary cancer (CRC) and 51 normal samples in The Cancer Genome Atlas Program (TCGA, https://cancergenome.nih.gov) were processed using the R package 'TCGAbiolinks' [21] as the training cohort (TCGA-COADREAD). The TCGA database was accessed to obtain MAF files of somatic mutation data based on whole-exome sequencing and CNA data. From the Gene Expression Omnibus (GEO; accession number: GSE17537; https://www.ncbi.nlm.nih.gov/geo/), the clinical data of 50 CRC patients and their gene expressions were collected for validation. Information on patients' clinical characteristics from the TCGA-COADREAD and GSE17537 datasets used is shown in Supplementary Table 1. The median expression value of genes with numerous probes was taken as the expression of the gene.

WGCNA analysis and key ICD-associated genes

ICD-related genes from a past study [22] were utilized to calculate ICD enrichment scores for each sample using the 'GSVA' package [23]. Co-expression network analysis was performed with the R package 'WGCNA' [24] under the soft thresholding at 3, which achieved a fit index of 0.85 to ensure a scale-free topology. Those with the highest enrichment score in ICD and the top 50% median absolute deviation in the expression profile were included in co-expression network analysis. Modules containing at least 30 genes were identified through hierarchical clustering. ICD-related modules were sectioned according to the correlation with the clinical data, and the pink and turquoise modules were selected. Furthermore, genes with high module membership (MM) and significance (GS) were considered as hub genes in each module (cor. gene GS > 0.6 and MM > 0.8).

Construction and evaluation of the ICDRS

Based on the expression value of the selected ICD-related modules, prognostic markers were identified using univariate Cox proportional hazard regressions (P-values < 0.05). Next, the ICDRS was developed with LASSO-penalized Cox regression. The LASSO penalty parameter λ was refined to determine the coefficient for each gene, and the ICDRS was formulated as follow:

$$\text{Score} = \sum_{i=0}^{n} \beta i * \chi i$$

where xi represented the expression of a gene and βi represented the gene's coefficient from the LASSO-penalized Cox regression model. Low-risk and high-risk patients were grouped by the median ICDRS value.

The correlation between clinical features and the ICDRS

Univariate Cox analysis was used to examine the correlation between clinical factors including gender, age, TNM stage, lymphatic invasion, risk scores, and patient survival

[25]. The independent prognostic value of the ICDRS was assessed by multivariate Cox proportional hazard regression. The clinical characteristics of the two risk groups were compared by the Wilcoxon rank-sum test.

Analyses of functional and pathway enrichment

Using the R package "clusterProfiler" [26, 27], Gene Ontology (GO) and Kyoto Encyclopedia of Genes and Genomes (KEGG) enrichment analyses were conducted. FDR-adjusted p-value < 0.05 was considered as statistically significant. To identify highly enriched gene sets (nominal p-values < 0.05 and FDR p-values < 0.05), 50 hallmark gene sets from the MSigDB were employed to perform gene set variation analysis (GSVA).

Estimating immune cell infiltration

Immune infiltration in each sample was measured utilizing the ssGSEA algorithm based on the expression level of markers specific to immune cells [28]. This approach was selected because ssGSEA does not rely on a reference dataset, making it suitable for RNA-seq data and enabling a comprehensive assessment of immune cell infiltration at the individual sample level. The resulting immune infiltration scores were further analyzed to explore their correlation with the ICDRS and their potential role in the tumor immune microenvironment of CRC. In addition, tumor purity, intratumoral, stromal and immune cell abundance of the tumor microenvironment were calculated by ESTIMATE based on gene expression profiles of the CRC tissues [29].

Genetic variation analysis

Genetic variation analysis was performed based on single nucleotide polymorphisms (SNPs) and copy number variations (CNVs) from the TCGA database. The mutation types and gene frequency were displayed applying the R21 "maftools" package [30]. CNA summary plots were visualized with the 'ggplot2' package in R to present chromosomal alterations. Circos plots were also plotted to show the distribution of ICD-

correlated genes utilizing the R package “RCircos” [31].

Drug sensitivity

The GDSC v2 (http://www.cancerrxgene.org) database stores cell line expression and drug response information and facilitates the correlation analysis between different drug responses and risk scores. The R package “OncoPredict” is a drug response prediction tool [32, 33]. The IC50 value refers to the concentration of a drug generally required to achieve its inhibitory effect, with a lower value indicating a higher cell sensitivity to the drug. The relationship between chemotherapy sensitivity and the risk score was examined by Spearman correlation analysis.

Cell culture and cell transfection

DMEM medium containing 1% antibiotic/antifungal solution and 10% fetal bovine serum (FBS) was used to culture the Caco2 (CRC cell line) and NCM460 (normal colonic mucosal epithelial cell line) purchased from the American Type Culture Collection (ATCC) at 37°C with 5% CO_2. Following the manufacturer's guidelines, Lipofectamine 2000 (Invitrogen, Carlsbad, CA, USA) was utilized for cell transfection. Briefly, Caco2 cells were seeded at a density of 2×10^5 cells per well in a 6-well plate and transfected with siRNA at a final concentration of 50 nM using 5 μL of Lipofectamine 2000 per well. To downregulate the *NRP1* gene, Caco2 cells were transfected with specific siRNA (si-*NRP1*#1: 5’-CAGCCTTGAATGCACTTATAT-3’ and si-*NRP1*#2: 5’-CAGAAGAATGGTACAAATCCAAG-3’, Sigma-Aldrich, St. Louis, MO, USA), while the controls were transfected with the corresponding non-specific control siRNA (si-NC, Sigma-Aldrich, St. Louis, MO, USA). After the transfection, the cells were cultured in an incubator for 48 hours (h) for subsequent experimental analysis.

Quantitative reverse transcriptase PCR (qRT-PCR)

Following the manufacturer's guidelines, TRIzol reagent (Invitrogen, Carlsbad, CA,

USA) was employed to separate total RNA, which was reverse-transcribed into cDNA using the PrimeScript RT kit (Takara Bio, Shiga, Japan). To quantify the expression levels of the *CLMP*, *PLEKHO* and *NRP1* genes, qRT-PCR analysis was performed with the use of SYBR Green PCR Master Mix (Applied Biosystems, Foster City, CA, USA) on an ABI 7500 real-time PCR system (Applied Biosystems, Foster City, CA, USA), strictly following the instructions. The primer sequences were listed as follows: *CLMP* Forward Sequence 5'-3': TCCTACTATGTTGGAACCTTGGG and Reverse Sequence 5'-3': CGGTGAGCAGCCATTCAATATC; *PLEKHO1* Forward Sequence 5'-3': GGGACCAGCTCTACATCTCTG and Reverse Sequence 5'-3': TGGAGTGGGCAAGAGTAAACT; *NRP1* Forward Sequence 5'-3': GGCGCTTTTCGCAACGATAAA and Reverse Sequence 5'-3': TCGCATTTTTCACTTGGGTGAT. *GAPDH* Forward Sequence 5'-3': GTCTCCTCTGACTTCAACAGCG and Reverse Sequence 5'-3': ACCACCCTGTTGCTGTAGCCAA.

CCK-8 assay

Caco2 cells at the logarithmic growth phase were plated into a 96-well plate with a density of 1×10^4 cells per well and incubated at 37°C with 5% CO_2 for durations of 0, 24, 48, or 72 hours. Subsequently, 10 μL of CCK-8 solution was introduced to the medium, and the samples were incubated at 37°C for 2 hours. To create the CCK-8 curve, absorbance readings at 450 nm were used on the Y-axis, while time was represented on the X-axis.

Wound healing test

A total of 4×10^5 Caco2 cells/well were suspended in 10 ml of medium and seeded into a 10-cm dish. When the cells reached 95% confluency, wounds on the cell layer were created using the tip of a 100 μl pipette (each wound had the same width). Subsequently, the scratches were washed with PBS solution, followed by incubating the samples in complete medium with 1% FBS at 37°C in 5% CO_2. The width of the scratches was

examined under an inverted microscope at both 0 and 48 h after the creation of the wounds. Images were analyzed using ImageJ v1.51n software.

Transwell assay

Cell invasion experiment was conducted using Matrigel (BD Biosciences, San Jose, CA, USA) to pre-coat the upper chambers (8.0 μm pore size, Corning Inc., Corning, NY, USA) of transwell. The transfected Caco2 cells (si-NRP1 and si-NC) were suspended in FBS-free DMEM and added to the upper chamber, while DMEM containing 20% FBS was added to the lower chamber as a chemoattractant. After incubation for 24-h, non-invading cells were removed from the upper chamber, and the cells invading into the lower chamber were fixed by 4% formaldehyde and dyed by 0.1% crystal violet. Cells penetrated the membrane were counted under a microscope (Olympus Corporation, Tokyo, Japan).

Statistical analysis

All the statistical studies were performed in the R language (https://www.R-project.org) or GraphPad Prism 8.0.2 (GraphPad., Inc., La Jolla, CA, USA). Prior to hypothesis testing, the normality of data distribution was assessed using the Shapiro-Wilk test. For normally distributed data, results were presented as mean ± standard deviation (SD), while for non-normally distributed data, results were expressed as median with interquartile range. Continuous variables between groups were compared using the Wilcoxon rank-sum test for non-normally distributed data and the Student's t-test for normally distributed data. The log-rank test is used to determine statistically significant differences in survival durations between groups under investigation. Independent prognostic factors associated with survival were identified by employing univariate and multivariate Cox proportional hazard regression analysis. ICD-related gene associations were assessed by Spearman correlation analysis. Unpaired t-test, one-way analysis of variance and two-way analysis of variance were applied during the statistical analyses of the experimental data. Statistical significance was set at p-values < 0.05. ns:

not significant (p-values > 0.05); * p-values < 0.05; ** p-values < 0.01; *** p-values < 0.001; **** p-values <0.0001.

RESULTS

ICD-related gene changes in CRC

A total of 34 genes involved in the ICD process were selected for further study based on a recent study [22]. Differential expression analysis showed that 82% (28/34) of these genes were significantly different in tumor tissue compared to normal samples in the TCGA-CRC cohort (Figure 1A), such as *CD8A*, *CD8B*, *CASP8*, *CASP1*, *CALR*, *HSP90AA1*, *IFNG*, *IFNGR1*, *PRF1*, *PIK3CA* and *TNF*. CRC patients were divided by TNM stage, lymphatic invasion, age, gender, and presence of perineural invasion. Comparison on the gene expressions showed that the levels of *CD8A, CASP1, IFNG,* and *IL17A* expressions were significantly downregulated in patients with stage III/IV than in stage I/II patients, suggesting an attenuated immune response in advanced tumors (Figure 1B). Additionally, we observed significant differences in the expression of *CASP1, ATG5, EIF2AK3, ENTPD,* and *IL17A* in lymphatic invasion patients and non-lymphatic invasion patients (Supplementary Figure 1A). Moreover, the expressions of *ENTPD1, IL1R1, LY96, MYD88,* and *NLRP3* in the perineural invasion presence group were significantly upregulated compared to those without perineural invasion (Supplementary Figure 1B). However, only a few genes were associated with age and gender in CRC (Supplementary Figure 1C, D). This was critical for understanding the immunomodulation of CRC and developing its specific therapeutic modalities.

The genome variation landscape of ICD-correlated genes was also examined. Overall, the ICD-correlated genes largely showed a low mutation frequency, except for PIK3CA, which primarily had missense mutations in 23% of the CRC samples (Figure 1C). This suggests that PIK3CA may influence immune escape and treatment response in CRC. Additionally, copy number amplification of IL6 may enhance the expression of pro-inflammatory factors, which in turn affects tumor progression and immunotherapeutic

response (Figure 1D). The pattern of variation in these genes suggests that ICD-related genes may play a critical role in cancer immunomodulation and may serve as potential biomarkers for predicting immunotherapeutic response.

Screening ICD-related gene modules based on WGCNA

WGCNA was conducted to section ICD-related key gene clusters. After the removal of outlier data, soft threshold ($\beta = 3$, scale-free $R2 = 0.850$) was used to ensure that the network was scale-free (Figure 2A) (Supplementary Figure 2A). Next, the correlations between the eigengenes of modules and the corresponding ICD score were calculated for CRC samples applying ssGSEA (Figure 2B, C). The pink and turquoise modules that exhibited higher correlations than other modules were selected for further analysis. Under the thresholds of cor. cor. GS > 0.6 and MM > 0.8, a total of 183 vital genes linked to ICD were screened (Figure 2D, E). Using Metascape, we performed protein-protein interactions (PPI) network analysis to further confirm the interactions among these genes (Supplementary Figure 2B). Function enrichment analysis of the biological processes of GO terms showed predominant enrichment in T cell activation, immune response-regulating signaling, immune response activation, and leukocyte proliferation (Supplementary Figure 2C), which was consistent with enriched cellular component and molecular function terms of the GO terms (Supplementary Figure 2D, E). KEGG pathway enrichment results also demonstrated that these genes were enriched to the immune-correlated functional pathways such as chemokine signaling and leukocyte transendothelial migration pathways (Supplementary Figure 2F).

Development of the prognostic signature ICDRS for CRC

To further screen key prognostic markers, we first identified seven key ICD-related genes, including *C5AR1*, *VIM*, *PLEKHO1*, *CSGALNACT2*, *NRP1*, *CLMP*, and *GPNMB,* using univariate cox regression analysis (Figure 3A). Next, we performed LASSO cox regression analysis on these genes to determine the optimal LASSO penalty parameter λ (Figure 3B, C) and substituted it into the ICDRS model. Ultimately, the three

prognostic genes, namely, *CLMP*, *NRP1*, and *PLEKHO1*, were used to build the ICDRS model (Figure 3D). According to the median gene expression levels of *CLMP*, *NRP1*, and *PLEKHO1,* high and low gene expression groups of the three genes were classified. As shown in Figure 3E-G, these genes were observed to be closely involved in the prognosis of CRC patients.

Evaluation and validation of ICDRS

In both the validation and training cohorts, the ICDRS scores were calculated and assessed. In comparison to those with low-risk scores (Figures 4A and B) (log-rank test, P-values < 0.05), the survival of patients with high-risk scores was more unfavorable. Additionally, neither group had any extreme or abnormal event in the distribution of risk score (Figure 4C, D). ICDRS was validated as an independent prediction indicator for the OS of CRC patients by univariate and multivariate Cox regression analyses (Figure 4E, F). These findings indicated that the ICDRS signature could be a novel prognostic indicator for patients with CRC.

ICDRS revealed the molecular characteristics and pathway alterations in CRC

To investigate the functional differences and molecular features of ICDRS, the ICDRS scores of patients were used to divide low-risk and high-risk groups. Compared with the low-risk patients, high-risk patients had higher mutation frequencies in *COL27A1* and *PTEN* (9% vs. 2% and 7% vs. 1%, respectively) than SNVs. In contrast, *COL7A1* mutation was more frequent in low-risk patients than those with a high risk (7% vs. 1%). Notably, most of them were missense mutations (Figure 5A, B). In addition, we found significant gene amplifications and deletions in several chromosomal regions in the high-risk group, while the low-risk group had an overall lower CNV frequency than the high-risk group (mean value of 0.68 in low-risk group vs. mean value of 0.70 in high-risk group, Figure 5C-E, Supplementary Table 2). We further calculated the activity of 50 cancer hallmark signatures in the TCGA-CRC cohort to examine the differences in the functional processes between the two groups. Substantial variations

in multiple cancer characteristics were found between the two risk groups (Figure 5F). The high-risk group had upregulated HYPOXIA, TGF-β SIGNALLING, APOPTOSIS, NOTCH signaling, and INTERFERON GAMMA RESPONSE, while the low-risk group had upregulated MYC targets including PEROXISOME. Thus, ICDRS was proven to be accurate in characterizing patients with different biological processes.

Immune infiltration profiles defined by ICDRS

ICDRS stratification was positively correlated with immune infiltration as the high-risk group had higher ESTIMATE, stromal, and immune scores, which indicated greater immune infiltration and lower tumor purity (Figure 6A-D). Complete analysis on the immune cell subtype revealed a high infiltration level of immune-suppressive cells such as T follicular helper and regulatory T cells in the high-risk group (Figure 6E) [34, 35]. The tumor mutation burden (Figure 6F, $R = 0.31$, $p = 7.4e{-}09$), T cell receptor (TCR) diversity (Figure 6G, $R = 0.5$, $p < 2.2e{-}16$), and cytolytic activity (Figure 6H, $R = 0.55$, $p < 2.2e{-}16$) were also strongly linked with the ICDRS score. Furthermore, the ICDRS score was also higher in the MSI-high group (Figure 6I, Wilcoxon rank-sum test, $p = 5e{-}04$). These findings demonstrated that immune suppression and anticancer immunity coexisted in the TME of CRC.

ICDRS-guided chemotherapy strategies

By stimulating ICD with specific chemotherapy agents, tumors can be more susceptible to checkpoint blockade therapies, but determining the optimal combination of chemotherapy and immunotherapy is the major difficulty [36, 37]. As the ICDRS was developed based on ICD-correlated genes, we speculated that ICDRS was potentially correlated with chemotherapy response. The 'oncoPredict' R software was employed to estimate the IC50 of pharmaceuticals. The Spearman correlation between log2-transformed IC50 of each drug and ICDRS risk score was calculated. The ICDRS risk score was negatively related to the sensitivity of AZ960_1250, AZD1332_1464, AZD8055_1059, ribociclib_1632, WZ4003_1614, and XAV939_1268 (Figure 7A).

Interestingly, AZ960, a novel Jak2 inhibitor, was reported to be effective in inducing apoptosis in cancer cells [38]. Conversely, the sensitivity of BI-2536_1086, dihydrorotenone_1827, SB5051_1194, SCH772984_1564, ulixertinib_1908, and ulixertinib_2047 were positively associated with the ICDRS risk score (Figure 7B), indicating their potential to serve as candidate drugs for treating cancer patients with different ICDRS scores. However, additional research should be performed to examine the correlation between ICDRS and drug susceptibility.

The expressions of characterized genes in CRC cells

To further validate the prognostic signatures we identified, we first detected the differences in the expression levels of *CLMP*, *PLEKHO*, and *NRP1* between CRC cells Caco2 and control cells (normal colonic mucosal cells NCM460) based on qRT-PCR and Western blotting. The mRNA expressions of *PLEKHO* and *NRP1* were significantly elevated as compared to normal colonic mucosal cells NCM460, whereas the expression of *CLMP* was significantly downregulated in cancer cells (Figure 8A). Consistently, the protein levels of these genes showed similar results (Figure 8B). It has been shown that *NRP1* is strongly associated with tumor progression and metastasis, and there is also a significant association with poorer patient survival in CRC [39]. For this reason, we selected the *NRP1* gene to verify the effect of its knockdown on the proliferation, migration and invasion levels of CRC cells (Figure 8C). The results of CCK-8 assay showed that knockdown of *NRP1* expression significantly reduced the proliferation level of CRC cells (Figure 8D). The migration and invasion of CRC cells were also remarkably inhibited after silencing *NRP1* expression (Figure 8E-F). These results revealed that prognostic markers screened on the basis of ICD-related genes had a potential impact on the occurrence and progression of CRC.

DISCUSSION

Advancements in treatment have been made; however, CRC remains a deadly disease with significant heterogeneity. This variability necessitates the optimization of

therapies to enhance survival rates and decrease mortality. Therefore, it is crucial to identify dependable prognostic biomarkers that can stratify survival risk and forecast therapeutic strategies tailored to specific subtypes. Li et al. used a multistep approach to construct a signature map based on immune-related genes using the TCGA and GEO databases, and found that CRC patients with low immune risk scores achieved better treatment outcomes with immunotherapy [40]. Zhao et al. delved into the molecular characterization of PANoptosis in CRC prognosis and constructed a prediction model based on four PANoptosis-related genes, namely *TIMP1*, *CDKN2A*, *CAMK2B* and *TLR3* [41]. ICDRS demonstrates a unique advantage over existing prognostic indicators in the prognostic assessment of CRC patients. As a novel type of regulated cell death, ICD has been shown to promote adaptive immunity and boost anti-tumor immune responses, suggesting that the identification of ICD-related biomarkers could help distinguish CRC patients who might benefit from immunotherapy [42]. Here, ICDRS is based on the expression of ICD-related genes that reflect complex changes in TME, which can more effectively identify high-risk patients who may require more aggressive treatment or immunotherapy, with greater predictive power and individualized treatment guidance value.

In this study, we first assessed the expression differences of ICD-correlated genes in both CRC and para-cancerous normal tissue samples based on public databases and analyzed the variants of ICD-related genes in the TCGA-CRC cohort. The intracellular mediator phosphatidylinositol-3-kinase (*PI3K*) (also known as gene symbol *PIK3CA*) functions crucially in the promoting cell transformation and proliferation, tumor initiation, and resistance to apoptosis. Stimulation of the activity of *e* occurs in the presence of external growth factors and hormones [43]. *PI3K* dysregulation triggers the activation of AKT, a serine/threonine kinase, in various types of cancers, ultimately influencing a variety of downstream proteins that stimulate unchecked cellular and tumor proliferation [44]. Approximately 15-20% of CRC is characterized by the presence of activating mutations in *PIK3CA*, which affects both the OS and progression-free survival of patients suffering from CRC [45]. In addition, *PIK3CA* mutations have different immune profiles in gastric cancer and can modulate tumor

immunogenicity [46]. Notably, we detected a high mutation frequency of *PIK3CA* in CRC samples based on the mutation profile of ICD-associated genes, indicating that *PIK3CA* mutations affected CRC growth and progression via DAMPs by altering the immune response of tumor to the immune system.

The ICDRS was developed for CRC by integrating univariate LASSO Cox regression analysis, Cox analysis, and WGCNA. The ICDRS showed a strong predictive significance in independently predicting the survival of CRC patients. The accuracy of the signature was validated using internal and multiple external validation datasets. Notably, many of the genes analyzed in our study have been previously linked to CRC. For instance, *C5AR1* is a master regulator in tumorigenesis of CRC through immune modulation [47]. After co-cultivation with the bacteria from CRC, the expression of *VIM* changes in Caco2 cells [48]. The prognostic significance and mechanism of *PLEKHO1* in the immune microenvironment of colon cancer have also been reported [49]. *PLEKHO1* contributes to the development of renal cell carcinoma, and its knockdown significantly can inhibit cancer cell viability and promote apoptosis [50]. *CLMP* is capable of regulating colon epithelial cell proliferation and preventing tumor growth [51]. *CLMP* has an anti-CRC effect and it can affect the resistance of CRC cells to all-trans retinoic acid [52]. Neuropilin-1 (*NRP1*), an important immunomodulatory receptor, has been found to be closely associated with the progression of CRC. The role of *NRP1* in TME is complex and involves both immunosuppression and is closely linked to angiogenesis [53]. *NRP1* inhibits anti-tumor immune responses by enhancing infiltration of regulatory T cells and promoting immune escape. [54]. In addition, *NRP1* activates the angiogenic pathway by interacting with vascular endothelial growth factor receptor 2 (VEGFR2), promoting nutrient supply to tumors, which in turn drives tumor growth and metastasis [55]. The current work was the first to demonstrate the effect of *NRP1* on CRC cell proliferation, migration and invasion based on ICD-related genes. Thus, *NRP1* is not only an important mediator of tumor immunomodulation, but also plays a key role in tumor angiogenesis. By targeting *NRP1*, it may help to restore the immune response and inhibit angiogenesis, providing a new strategy for immunotherapy and antitumor therapy.

CRC is often associated with chronic inflammation [56]. Inflammation in the gastrointestinal tract triggers cancer-causing genetic changes and initiates the development of CRC. Furthermore, immune cells such as myeloid and lymphoid cells infiltrate the existing tumors and drive "inflammation provoked by tumors", leading to cancer growth by promoting the survival and growth of cancerous cells [57, 58]. Here, we identified two ICDRS subtypes with distinct TME landscapes. Increased infiltration of different immune cells was found to be related to a higher ICDRS, indicating the coexistence of pro- and anti-tumor components in the TME. The presence of activated CD4+ T cells and active CD8+ T cells in CRC patients is closely associated with antitumor immunity [59, 60]. Follicular T helper cells are also related to the survival of patients with CRC [61]. Moreover, Th17-type cytokines activate *STAT3* and NF-kB pathway to promote CRC tumorigenesis [62]. Due to the coexistence of immunological activation and immune suppression, immune-related characteristics enriched in the group with a high ICDRS score were identified by GSVA. In comparison to patients with low ICDRS scores, those with high ICDRS scores will benefit more from checkpoint inhibitors as they showed higher levels of these immune checkpoints.

Limitations

Apart from these promising findings, the present work also had some limitations. The study of the relationship between ICDRS and the therapeutic sensitivity of anti-PD-L1 was hindered by a lack of data from CRC patients with ICB treatment. To better elucidate the molecular mechanisms underlying CRC immunobiology, further studies are encouraged to validate the prognostic value of ICRDS in larger datasets with multi-omics analysis. Additionally, transcriptomic analysis might also benefit from integrating proteomics and metabolomics. In particular, the mechanism of action of the screened prognostic genes in CRC should be further validated by performing experiments such as mouse xenograft models or knockout models.

CONCLUSION

This study established and validated a robust ICD-correlated prognostic signature that can accurately predict the survival outcomes and reveal distinct immune statutes and molecular features between the two risk groups of CRC. Further exploration and validation are needed to probe into the therapeutic implications of the current signature in CRC.

ACKNOWLEDGMENT

The authors thank Beijing GAP Biotechnology Co.Ltd. for their support in this study.

Funding: The study was supported by Classification of cfDNA methylation drivers in colorectal cancer Signature construction and personalized screening of potential therapeutic drugs (No. Dr202309).

Conflicts of interest: The authors declared no conflicts of interest.

Data availability statement: The datasets analyzed herein are publicly available at the Gene Expression Omnibus (GSE17537) (https://www.ncbi.nlm.nih.gov/geo/GSE17537) and TCGA (https://portal.gdc.cancer.gov/) databases.

Submitted: 9 January 2025

Accepted: 5 April 2025

Published online: April 2025

REFERENCES

1. Klimeck L, Heisser T, Hoffmeister M, Brenner H. Colorectal cancer: A health and economic problem. Best practice & research Clinical gastroenterology. 2023;66:101839.
2. Ruan Y, Lu G, Yu Y, Luo Y, Wu H, Shen Y, et al. PF-04449913 Inhibits Proliferation and Metastasis of Colorectal Cancer Cells by Down-regulating MMP9 Expression through the ERK/p65 Pathway. Current Molecular Pharmacology. 2023;17.
3. Kleppe A, Albregtsen F, Vlatkovic L, Pradhan M, Nielsen B, Hveem TS, et al. Chromatin organisation and cancer prognosis: a pan-cancer study. Lancet Oncol. 2018;19(3):356-69.

4. Li M, Fan J, Hu M, Xu J, He Z, Zeng J. Quercetin Enhances 5-fluorouracil Sensitivity by Regulating the Autophagic
Flux and Inducing Drp-1 Mediated Mitochondrial Fragmentation in Colorectal
Cancer Cells. Current Molecular Pharmacology. 2024;17.
5. Pourhanifeh MH, Vosough M, Mahjoubin-Tehran M, Hashemipour M, Nejati M, Abbasi-Kolli M, et al. Autophagy-related microRNAs: Possible regulatory roles and therapeutic potential in and gastrointestinal cancers. Pharmacol Res. 2020;161:105133.
6. Shafabakhsh R, Arianfar F, Vosough M, Mirzaei HR, Mahjoubin-Tehran M, Khanbabaei H, et al. Autophagy and gastrointestinal cancers: the behind the scenes role of long non-coding RNAs in initiation, progression, and treatment resistance. Cancer Gene Ther. 2021;28(12):1229-55.
7. Salleh EA, Lee YY, Zakaria AD, Jalil NAC, Musa M. Cancer-associated fibroblasts of colorectal cancer: Translational prospects in liquid biopsy and targeted therapy. Biocell. 2023;47(10):2233-44.
8. Garg AD, Dudek-Peric AM, Romano E, Agostinis P. Immunogenic cell death. Int J Dev Biol. 2015;59(1-3):131-40.
9. Galluzzi L, Vitale I, Warren S, Adjemian S, Agostinis P, Martinez AB, et al. Consensus guidelines for the definition, detection and interpretation of immunogenic cell death. J Immunother Cancer. 2020;8(1).
10. Legrand AJ, Konstantinou M, Goode EF, Meier P. The Diversification of Cell Death and Immunity: Memento Mori. Molecular cell. 2019;76(2):232-42.
11. Galluzzi L, Vitale I, Aaronson SA, Abrams JM, Adam D, Agostinis P, et al. Molecular mechanisms of cell death: recommendations of the Nomenclature Committee on Cell Death 2018. Cell death and differentiation. 2018;25(3):486-541.
12. Ahmed A, Tait SWG. Targeting immunogenic cell death in cancer. Mol Oncol. 2020;14(12):2994-3006.
13. Cai J, Hu Y, Ye Z, Ye L, Gao L, Wang Y, et al. Immunogenic cell death-related risk signature predicts prognosis and characterizes the tumour microenvironment in lower-grade glioma. Front Immunol. 2022;13:1011757.
14. Wang X, Wu S, Liu F, Ke D, Wang X, Pan D, et al. An Immunogenic Cell Death-Related Classification Predicts Prognosis and Response to Immunotherapy in Head and Neck Squamous Cell Carcinoma. Front Immunol. 2021;12:781466.
15. Tian Z, Zhang P, Li X, Jiang D. Analysis of immunogenic cell death in ascending thoracic aortic aneurysms based on single-cell sequencing data. Front Immunol. 2023;14:1087978.
16. Alzeibak R, Mishchenko TA, Shilyagina NY, Balalaeva IV, Vedunova MV, Krysko DV. Targeting immunogenic cancer cell death by photodynamic therapy: past, present and future. J Immunother Cancer. 2021;9(1).
17. Krysko DV, Vandenabeele P. Clearance of dead cells: mechanisms, immune responses and implication in the development of diseases. Apoptosis. 2010;15(9):995-7.
18. Zheng ML, Liu XY, Han RJ, Yuan W, Sun K, Zhong JC, et al. Circulating exosomal long non-coding RNAs in patients with acute myocardial infarction. Journal of cellular and molecular medicine. 2020;24(16):9388-96.

19. Galluzzi L, Buque A, Kepp O, Zitvogel L, Kroemer G. Immunogenic cell death in cancer and infectious disease. Nat Rev Immunol. 2017;17(2):97-111.
20. Liu P, Zhao L, Pol J, Levesque S, Petrazzuolo A, Pfirschke C, et al. Crizotinib-induced immunogenic cell death in non-small cell lung cancer. Nat Commun. 2019;10(1):1486.
21. Colaprico A, Silva TC, Olsen C, Garofano L, Cava C, Garolini D, et al. TCGAbiolinks: an R/Bioconductor package for integrative analysis of TCGA data. Nucleic Acids Res. 2016;44(8):e71.
22. Garg AD, De Ruysscher D, Agostinis P. Immunological metagene signatures derived from immunogenic cancer cell death associate with improved survival of patients with lung, breast or ovarian malignancies: A large-scale meta-analysis. Oncoimmunology. 2016;5(2):e1069938.
23. Charoentong P, Finotello F, Angelova M, Mayer C, Efremova M, Rieder D, et al. Pan-cancer Immunogenomic Analyses Reveal Genotype-Immunophenotype Relationships and Predictors of Response to Checkpoint Blockade. Cell Rep. 2017;18(1):248-62.
24. Langfelder P, Horvath S. WGCNA: an R package for weighted correlation network analysis. BMC Bioinformatics. 2008;9:559.
25. Kawai S, Kido T, Teguri Y, Miwa K, Kanaya T, Ishii Y, et al. Long-Term Outcomes of Systemic-to-Pulmonary Artery Shunt in Patients with Functional Single Ventricle and Heterotaxy Syndrome. Congenital Heart Disease. 2023;18(4):399-411.
26. Yu G, Wang LG, Han Y, He QY. clusterProfiler: an R package for comparing biological themes among gene clusters. Omics : a journal of integrative biology. 2012;16(5):284-7.
27. Chen J, Lin A, Luo P. Advancing pharmaceutical research: A comprehensive review of cutting-edge tools and technologies. Current Pharmaceutical Analysis. 2024;21(1):1-19.
28. Subramanian A, Tamayo P, Mootha VK, Mukherjee S, Ebert BL, Gillette MA, et al. Gene set enrichment analysis: a knowledge-based approach for interpreting genome-wide expression profiles. Proc Natl Acad Sci U S A. 2005;102(43):15545-50.
29. Yoshihara K, Shahmoradgoli M, Martinez E, Vegesna R, Kim H, Torres-Garcia W, et al. Inferring tumour purity and stromal and immune cell admixture from expression data. Nat Commun. 2013;4:2612.
30. Mayakonda A, Lin DC, Assenov Y, Plass C, Koeffler HP. Maftools: efficient and comprehensive analysis of somatic variants in cancer. Genome Res. 2018;28(11):1747-56.
31. Zhang H, Meltzer P, Davis S. RCircos: an R package for Circos 2D track plots. BMC Bioinformatics. 2013;14:244.
32. Maeser D, Gruener RF, Huang RS. oncoPredict: an R package for predicting in vivo or cancer patient drug response and biomarkers from cell line screening data. Brief Bioinform. 2021;22(6).
33. Liu Y, Zhang S, Liu K, Hu X, Gu X. Advances in drug discovery based on network pharmacology and omics technology. Current Pharmaceutical Analysis. 2024;21(1):33-43.

34. Overacre-Delgoffe AE, Bumgarner HJ, Cillo AR, Burr AHP, Tometich JT, Bhattacharjee A, et al. Microbiota-specific T follicular helper cells drive tertiary lymphoid structures and anti-tumor immunity against colorectal cancer. Immunity. 2021;54(12):2812-24 e4.
35. Zou W. Regulatory T cells, tumour immunity and immunotherapy. Nat Rev Immunol. 2006;6(4):295-307.
36. Patel SA, Minn AJ. Combination Cancer Therapy with Immune Checkpoint Blockade: Mechanisms and Strategies. Immunity. 2018;48(3):417-33.
37. Upadhaya S, Neftelino ST, Hodge JP, Oliva C, Campbell JR, Yu JX. Combinations take centre stage in PD1/PDL1 inhibitor clinical trials. Nat Rev Drug Discov. 2021;20(3):168-9.
38. Yang J, Ikezoe T, Nishioka C, Furihata M, Yokoyama A. AZ960, a novel Jak2 inhibitor, induces growth arrest and apoptosis in adult T-cell leukemia cells. Molecular cancer therapeutics. 2010;9(12):3386-95.
39. Fernández-Palanca P, Payo-Serafín T, Fondevila F, Méndez-Blanco C, San-Miguel B, Romero MR, et al. Neuropilin-1 as a Potential Biomarker of Prognosis and Invasive-Related Parameters in Liver and Colorectal Cancer: A Systematic Review and Meta-Analysis of Human Studies. Cancers. 2022;14(14).
40. Li Y, Li Y, Xia Z, Zhang D, Chen X, Wang X, et al. Identification of a novel immune signature for optimizing prognosis and treatment prediction in colorectal cancer. Aging. 2021;13(23):25518-49.
41. Zhao T, Zhang X, Liu X, Jiang X, Chen S, Li H, et al. Characterizing PANoptosis gene signature in prognosis and chemosensitivity of colorectal cancer. Journal of gastrointestinal oncology. 2024;15(5):2129-44.
42. Galluzzi L, Guilbaud E, Schmidt D, Kroemer G, Marincola FM. Targeting immunogenic cell stress and death for cancer therapy. Nat Rev Drug Discov. 2024;23(6):445-60.
43. Reinhardt K, Stückrath K, Hartung C, Kaufhold S, Uleer C, Hanf V, et al. PIK3CA-mutations in breast cancer. Breast cancer research and treatment. 2022;196(3):483-93.
44. Miricescu D, Totan A, Stanescu S, II, Badoiu SC, Stefani C, Greabu M. PI3K/AKT/mTOR Signaling Pathway in Breast Cancer: From Molecular Landscape to Clinical Aspects. International journal of molecular sciences. 2020;22(1).
45. Mei ZB, Duan CY, Li CB, Cui L, Ogino S. Prognostic role of tumor PIK3CA mutation in colorectal cancer: a systematic review and meta-analysis. Annals of oncology : official journal of the European Society for Medical Oncology. 2016;27(10):1836-48.
46. Choi S, Kim H, Heo YJ, Kang SY, Ahn S, Lee J, et al. PIK3CA mutation subtype delineates distinct immune profiles in gastric carcinoma. The Journal of pathology. 2023;260(4):443-54.
47. Ding P, Li L, Li L, Lv X, Zhou D, Wang Q, et al. C5aR1 is a master regulator in Colorectal Tumorigenesis via Immune modulation. Theranostics. 2020;10(19):8619-32.
48. Wachsmannova L, Stevurkova V, Ciernikova S. Changes in SNAI1 and VIM gene expression in Caco2 cells after cocultivation with bacteria from colorectal cancer biopsies. Neoplasma. 2019;66(2):271-5.

49. Wang X, Duanmu J, Fu X, Li T, Jiang Q. Analyzing and validating the prognostic value and mechanism of colon cancer immune microenvironment. J Transl Med. 2020;18(1):324.
50. Yu Z, Li Q, Zhang G, Lv C, Dong Q, Fu C, et al. PLEKHO1 knockdown inhibits RCC cell viability in vitro and in vivo, potentially by the Hippo and MAPK/JNK pathways. International journal of oncology. 2019;55(1):81-92.
51. Luissint AC, Fan S, Nishio H, Lerario AM, Miranda J, Hilgarth RS, et al. CXADR-Like Membrane Protein Regulates Colonic Epithelial Cell Proliferation and Prevents Tumor Growth. Gastroenterology. 2024;166(1):103-16.e9.
52. Wu Z, Zhang X, An Y, Ma K, Xue R, Ye G, et al. CLMP is a tumor suppressor that determines all-trans retinoic acid response in colorectal cancer. Developmental cell. 2023;58(23):2684-99.e6.
53. Dong Y, Ma WM, Shi ZD, Zhang ZG, Zhou JH, Li Y, et al. Role of NRP1 in Bladder Cancer Pathogenesis and Progression. Front Oncol. 2021;11:685980.
54. Chuckran CA, Liu C, Bruno TC, Workman CJ, Vignali DA. Neuropilin-1: a checkpoint target with unique implications for cancer immunology and immunotherapy. J Immunother Cancer. 2020;8(2).
55. Sharma S, Ehrlich M, Zhang M, Blobe GC, Henis YI. NRP1 interacts with endoglin and VEGFR2 to modulate VEGF signaling and endothelial cell sprouting. Communications biology. 2024;7(1):112.
56. Li SC, Lin HP, Chang JS, Shih CK. Lactobacillus acidophilus-Fermented Germinated Brown Rice Suppresses Preneoplastic Lesions of the Colon in Rats. Nutrients. 2019;11(11).
57. Chen J, Pitmon E, Wang K. Microbiome, inflammation and colorectal cancer. Seminars in immunology. 2017;32:43-53.
58. Shahrajabian MH, Sun W. Survey on Multi-omics, and Multi-omics Data Analysis, Integration and
Application. Current Pharmaceutical Analysis. 2023;19(4):267-81.
59. Shang S, Yang YW, Chen F, Yu L, Shen SH, Li K, et al. TRIB3 reduces CD8(+) T cell infiltration and induces immune evasion by repressing the STAT1-CXCL10 axis in colorectal cancer. Sci Transl Med. 2022;14(626):eabf0992.
60. Toor SM, Murshed K, Al-Dhaheri M, Khawar M, Abu Nada M, Elkord E. Immune Checkpoints in Circulating and Tumor-Infiltrating CD4(+) T Cell Subsets in Colorectal Cancer Patients. Front Immunol. 2019;10:2936.
61. Mo X, Huang X, Feng Y, Wei C, Liu H, Ru H, et al. Immune infiltration and immune gene signature predict the response to fluoropyrimidine-based chemotherapy in colorectal cancer patients. Oncoimmunology. 2020;9(1):1832347.
62. De Simone V, Franze E, Ronchetti G, Colantoni A, Fantini MC, Di Fusco D, et al. Th17-type cytokines, IL-6 and TNF-alpha synergistically activate STAT3 and NF-kB to promote colorectal cancer cell growth. Oncogene. 2015;34(27):3493-503.

FIGURES WITH LEGENDS

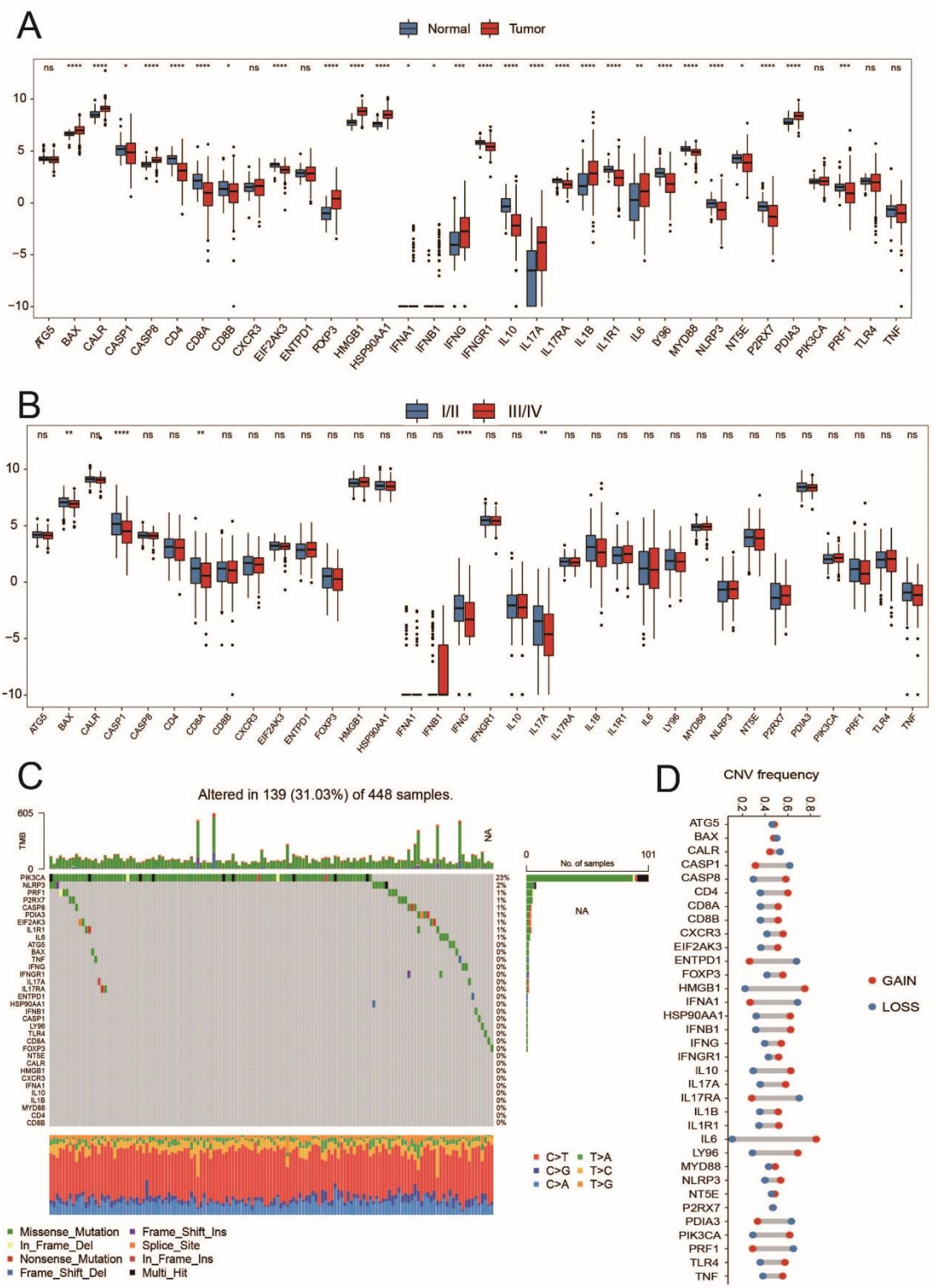

Figure 1. Genetic landscape of ICD-related genes

(A) Genes related to ICD between tumor and normal samples were subjected to

differential expression analysis. (B) Between stage I/II and III/IV samples, differential expression analysis on the ICD-correlated genes with differences was performed. (C) Mutation landscape of ICD-correlated genes in the TCGA-CRC cohort. (D) CNV frequencies of ICD-correlated genes.

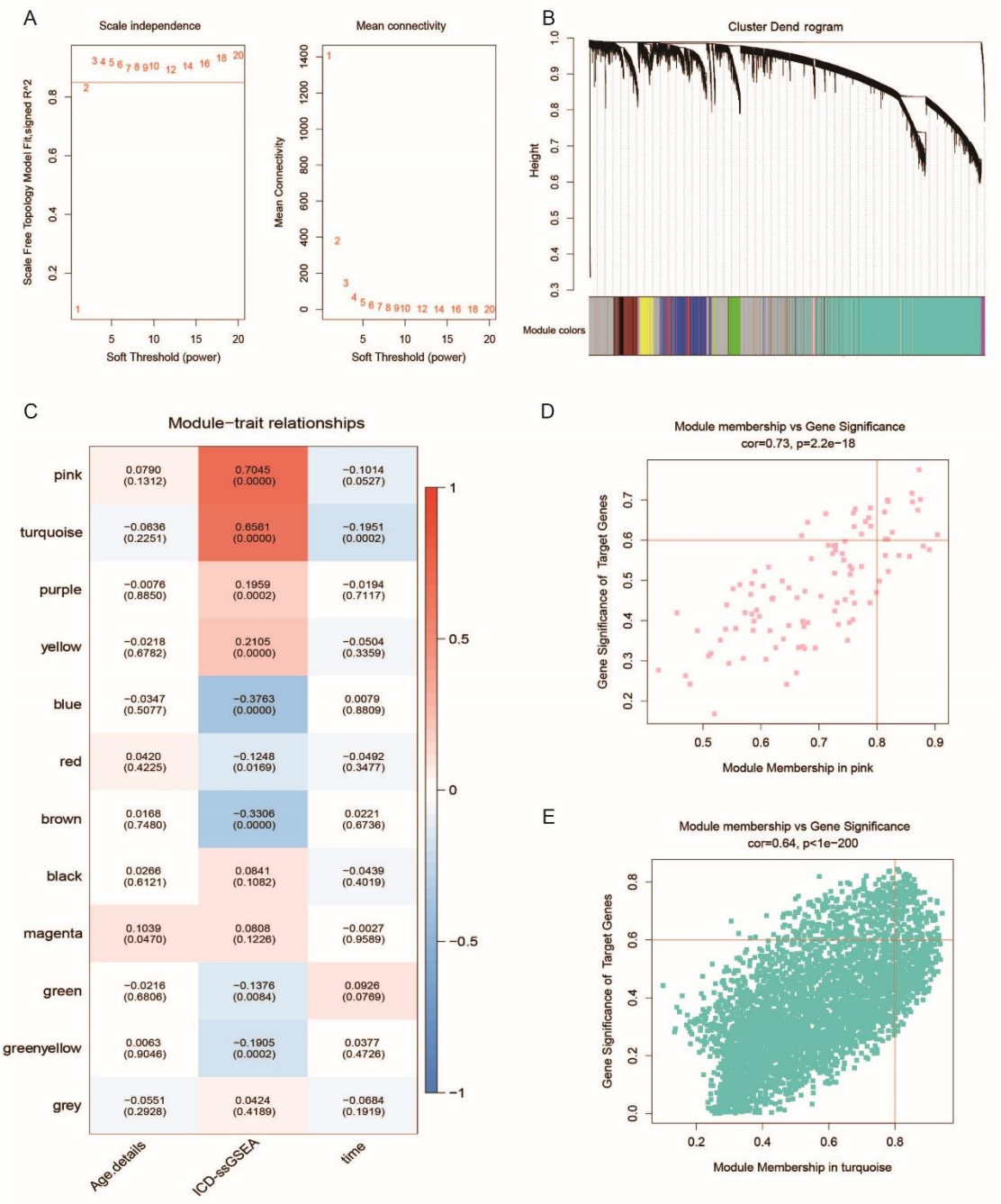

Figure 2. ICD-related key gene screening

(A) Scale-free fit index analyses of network topologies for various soft-thresholding

powers. (B) Gene clustering dendrogram based on topological overlaps. Various modules were assigned different colors. (C) Module and clinical trait correlation study. MM and GS correlation analysis. Correlation analysis using scatter plots of the pink and (D) turquoise modules (E).

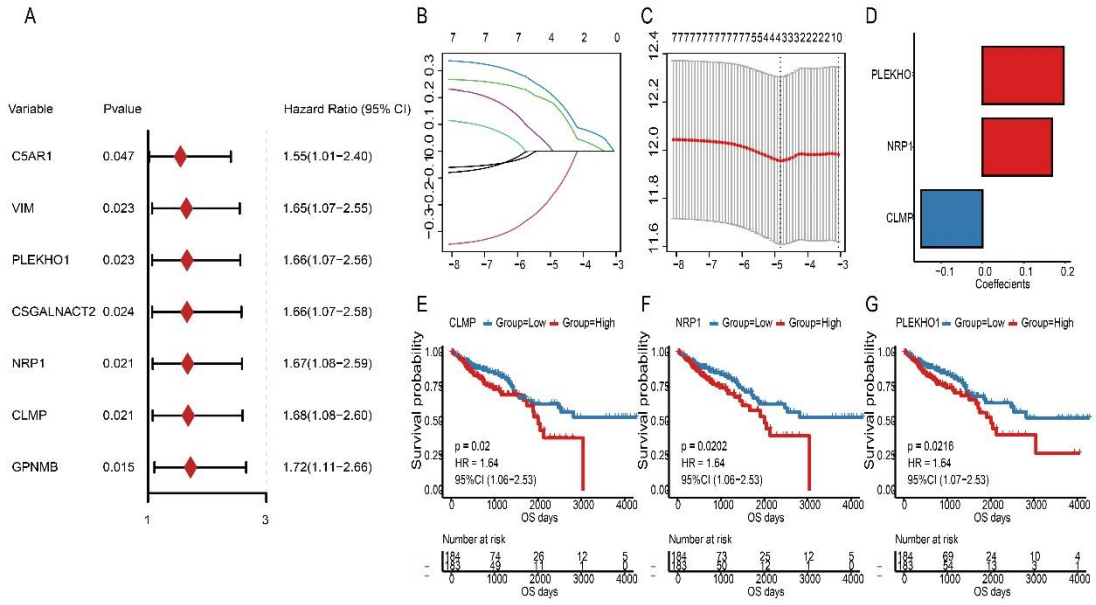

Figure 3. ICD-related genes with prognostic significance

(A) The univariate Cox regression analysis of ICD-related genes was presented as forest plot. (B) LASSO regression complexity controlled by the lambda. (C) LASSO regression confidence intervals of λ. (D) LASSO regression coefficients of the three key prognostic genes. (E-G) According to the expressions of key prognostic genes, the OS in low and high expression groups was visually compared according to Kaplan-Meier curves.

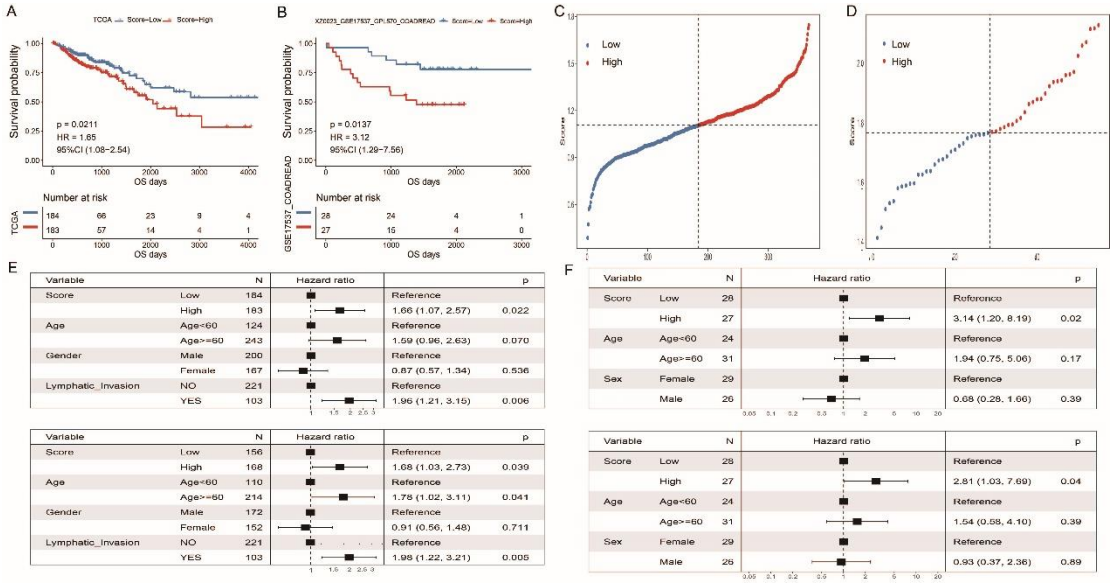

Figure 4. Evaluation and validation of ICDRS.

Kaplan-Meier curves of OS between the low-risk and high-risk groups based on the median ICDRS in the TCGA-CRC cohort. (B) According to the median ICDRS value in the validation cohort, Kaplan-Meier curves of OS were plotted for the two risk groups. (C) Risk score distribution in the TCGA-CRC cohort. (D) Risk score distribution in the validation cohort. (E) Univariate and multivariate Cox regression analyses to calculate risk score for TCGA-CRC patients. (F) Using univariate and multivariate Cox regression analyses for assessing the risk scores in validation cohort.

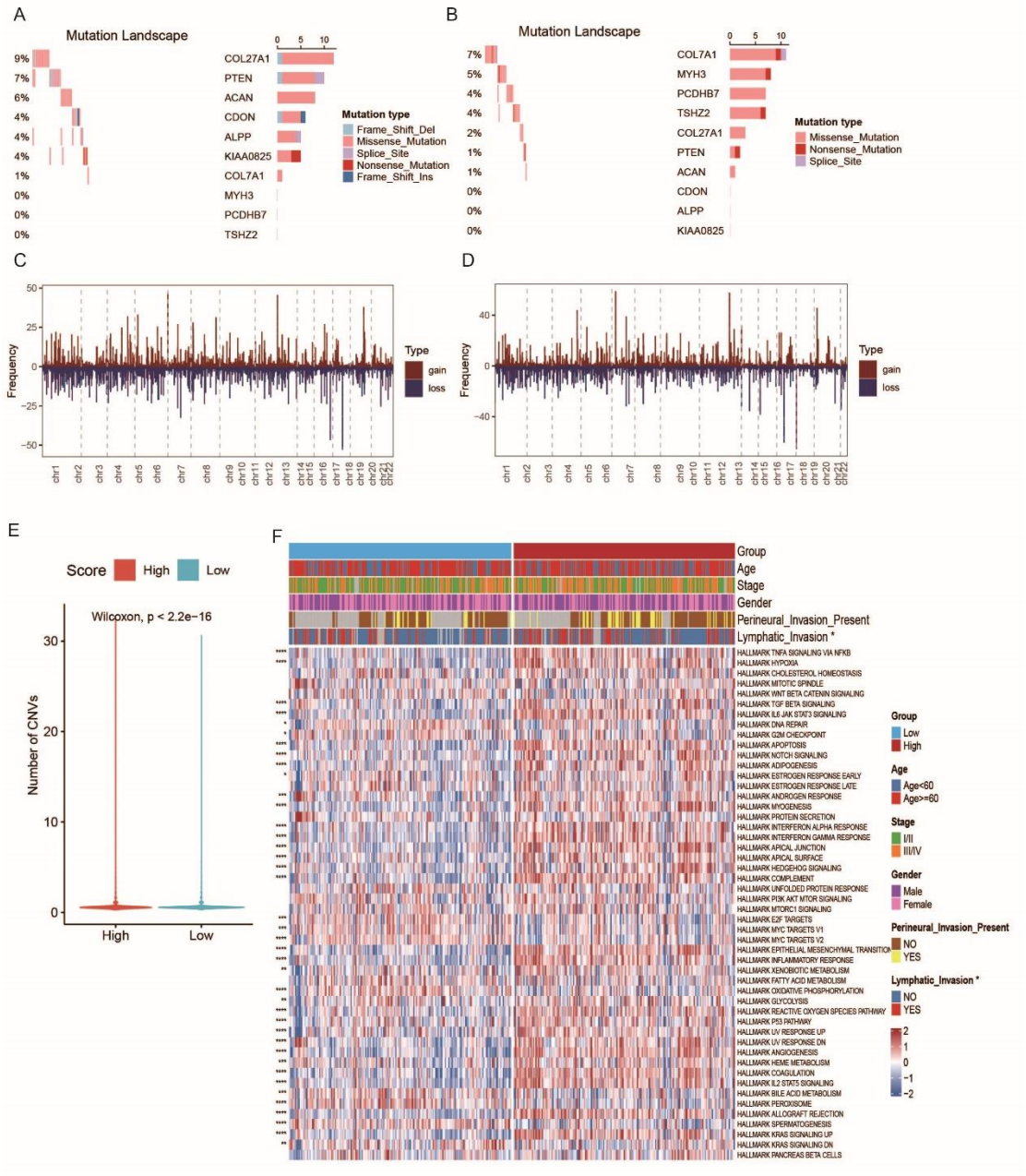

Figure 5. Association between the ICDRS signature and molecular traits

(A) The 10 most frequently mutated genes in the high-risk group were displayed in an oncoplot. (B) The 10 most frequently mutated genes in the low-risk group were displayed in an oncoplot. (C) Variations in copy numbers in the high-risk group. (D) Copy number variations in the low-risk group. (E) The distribution of copy number variations between the two risk groups. (F) Heatmap of the 50 signature pathway activity scores between the two risk groups.

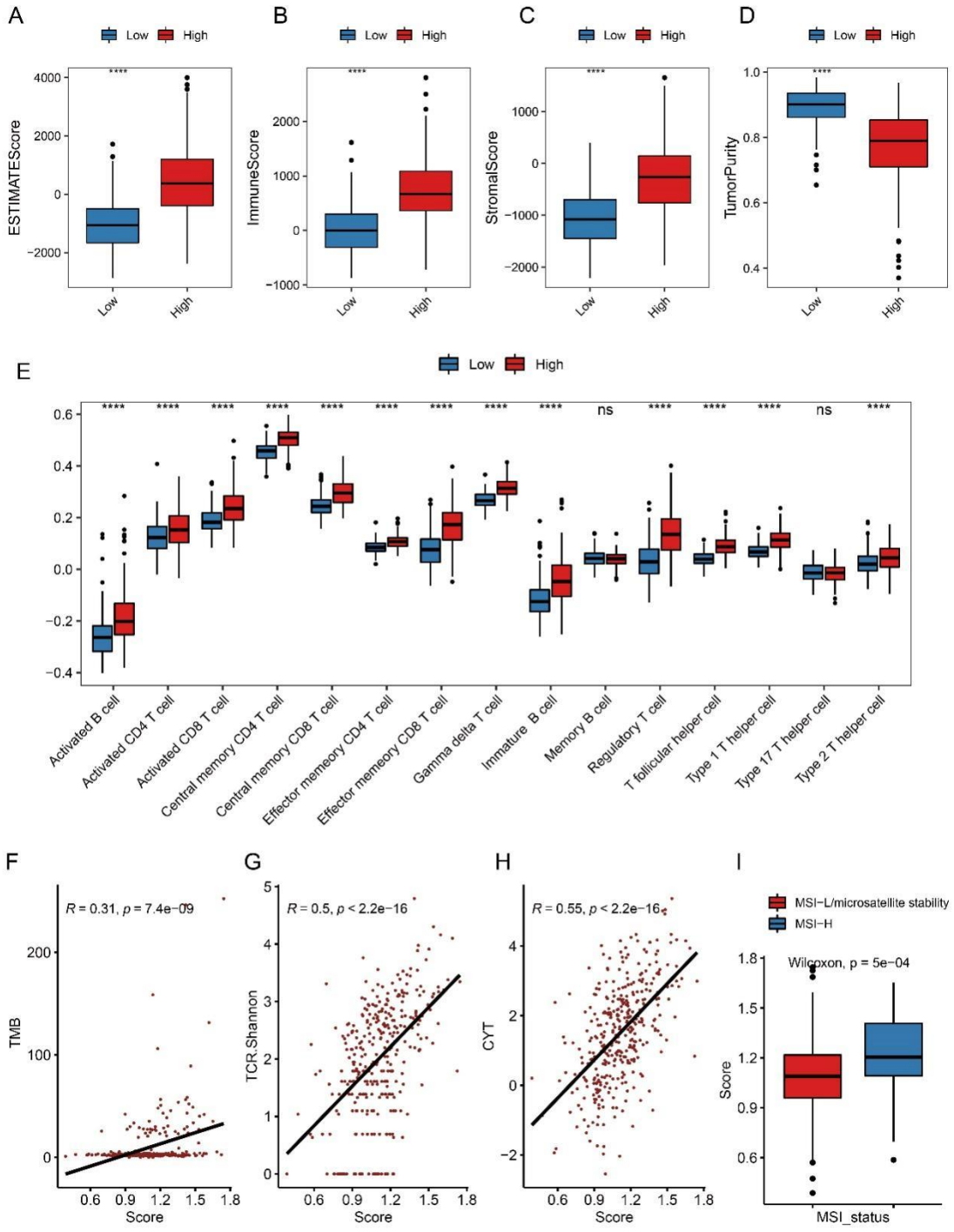

Figure 6. The tumor immune microenvironment and immunogenomic characteristics of CRC related to the ICDRS

ESTIMATE score comparison (A), immune score (B), stromal score (C), and tumor purity (D) calculated using ESTIMATE between the high- and low-risk groups. (E)

Comparison of the immune cell abundances between the two risk groups. Spearman correlation between the ICDRS risk score and tumor mutation burden (F), TCR diversity (G), and cytolytic activity (H). (I) ICDRS risk score distribution in the MSI-high and MSI-stability cohorts. To determine significance, the Wilcoxon rank-sum test was utilized. 'ns': P-values > 0.05, '*': P-values < 0.05, '**': P-values < 0.01, '***': P-values < 0.001, and '****': P-values < 0.0001.

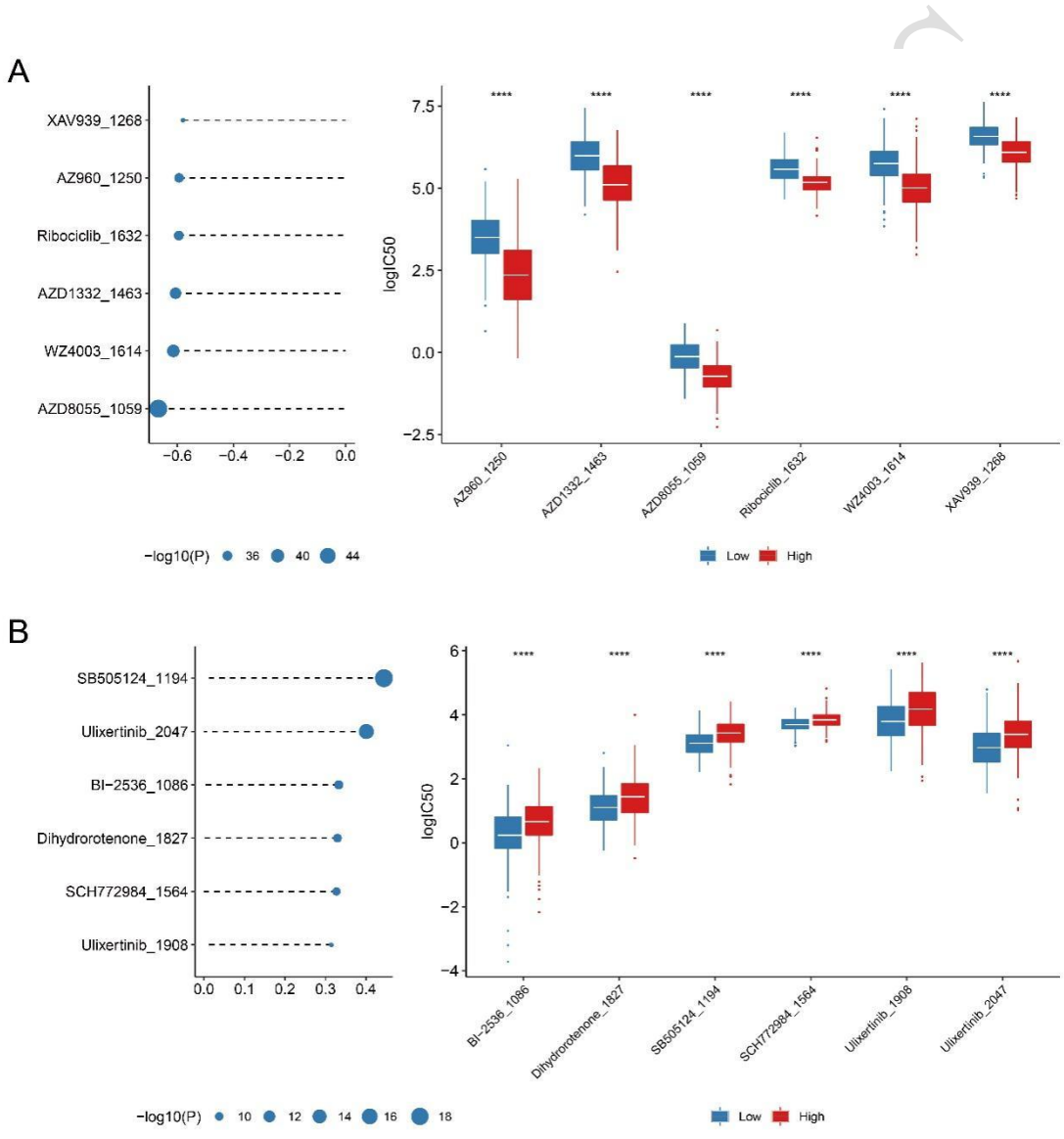

Figure 7. Correlation of the sensitivity of drugs with ICDRS signature

(A) Top six agents negatively associated with ICDRS. (B) Top six agents positive associated with ICDRS.

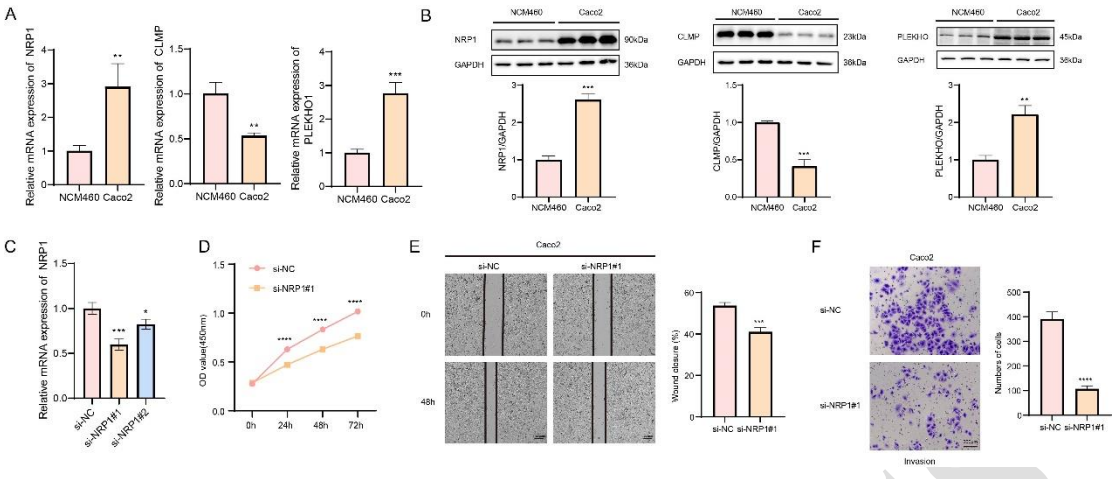

Figure 8. The role of ICDRS signature on the biological function of CRC cells

(A) The mRNA expression levels of *NRP1*, *CLMP*, and *PLEKHO* in NCM460 and Caco2 cells, respectively. (B) The protein expression levels of *NRP1*, *CLMP*, and *PLEKHO* in NCM460 and Caco2 cells, respectively. (C) Based on qRT-PCR to verify the efficiency of *NRP1* knockdown (si-*NRP1*#1 and si-*NRP1*#2). (D) CCK-8 assay to verify the effect of *NRP1* knockdown on the proliferative capacity of CRC cells. (E) Wound healing assay to assess the effect of *NRP1* on the migration of CRC cells. (F) Transwell assay to assess the ability of *NRP1* knockdown to inhibit invasion of CRC cells. All procedures were subjected to three independent repetitive tests. '∗': P-values < 0.05, '∗∗': P-values < 0.01, '∗∗∗': P-values < 0.001, and '∗∗∗∗': P-values < 0.0001.

SUPPLEMENTAL DATA

Supplementary data are available at the following links:

https://www.bjbms.org/ojs/index.php/bjbms/article/view/12028/3834

https://www.bjbms.org/ojs/index.php/bjbms/article/view/12028/3835